DEVELOPMENT OF A FINITE ELEMENT MODEL
FOR A BUCKLING RESTRAINED BRACE

Ciprian Ionut ZUB[1], Aurel STRATAN[1], Adrian DOGARIU[1], Dan DUBINA[1,2]

[1] Politehnica University of Timisoara, Department of Steel Structures and Structural Mechanics, Timisoara, Romania
[2] Romanian Academy, Fundamental and Advanced Technical Research Centre, Timisoara, Romania
Corresponding author: Ciprian Ionut ZUB, E-mail: `ciprian.zub@student.upt.ro`

Abstract. Buckling Restrained Braces (BRBs) have been used for more than 30 years as structural fuse elements due to their enhanced features when compared to conventional braces: no buckling in compression, stable and quasi-symmetric cyclic response, capacity to dissipate a large amount of energy. To achieve these performances, BRBs are composed of a steel core with variable cross-section that undergoes plastic deformations, and a buckling restraining mechanism that restrains the lateral displacements of the core, thus allowing it to achieve higher buckling modes in compression. The two components are decoupled by an unbonding interface which can be either a material layer, or a small gap. The use of BRBs in Romania is regulated by the seismic design code P100-1/2013, which requires experimental qualification. To overcome this problem, a set of typical BRBs with capacities corresponding to typical steel multi-storey buildings in Romania were tested and qualified at CEMSIG Laboratory. This paper presents the development of a numerical model for the tested BRBs in Abaqus software by using the Finite Element Method (FEM). The calibration of the material model, geometrical nonlinearities, and contact law based on experimental data are presented in detail.

Key words: BRB, calibration, FEM, qualification.

1. INTRODUCTION

The development of BRBs started in Japan in the 1970's, initially as steel braces restrained by concrete panels against buckling (Yoshino et al. (1971) in [1]), and, later, as steel braces restrained against buckling by a compact buckling restraining mechanism (Kimura et al. (1976) in [1]). The later concept was further developed by other researchers [2] due to its cyclic performance. Conceptually, a BRB consists of a dissipative steel core encased in a buckling restraining mechanism (BRM) that confines the core, preventing global buckling. The core is decoupled from the BRM by using an unbonding interface (material or gap), allowing it to achieve higher compression modes. Depending on the type of the BRM, the BRBs can be "conventional" (BRM is a concrete-filled steel tube) or "dry" (BRM is a steel assembly).

Throughout the years, BRBs have been extensively developed, tested and patented in Japan, USA, Canada, Taiwan [1]. In Europe, just few tests were performed up to date [3, 4, 5]. The use of BRBs in Europe is not regulated by Eurocode 8 [6] yet. However, general design rules, as well as manufacturing and testing requirements of BRBs are available in EN 15129 [7]. The national anti-seismic design code of Romania, P100-1/2013 [8], introduced provisions for design of steel structures with BRBs since January 2014. The code requires experimental qualification of BRBs used in practical applications, either project-specific, or based on existing experimental evidence. To overcome this problem, a set of typical BRBs with capacities (N_{pl}) corresponding to typical low-rise (N_{pl} = 300 kN) and mid-rise (N_{pl} = 700 kN) multi-storey buildings in Romania were tested and qualified at CEMSIG Laboratory [9]. The experimental qualification was done based on P100-1/2013 [8] and ANSI/AISC 341-10 [10] provisions.

This paper presents the development of a numerical finite element model (FEM) capable of simulating the cyclic behaviour of the tested BRBs. The development and the calibration of the BRB FEM model were performed using Abaqus software.

2. SUMMARY OF EXPERIMENTAL RESULTS

The experimental program consisted of 14 BRB tests, 10 "conventional" and 4 "dry". Further details regarding the experimental tests are presented in [9]. Within this paper the "conventional" BRB solutions are investigated, since they demonstrated a good cyclic performance and were easier to fabricate in comparison to "dry" BRB solutions.

The tested "conventional" BRBs were of two types (Fig. 1): type A and type B. Both typologies consisted of a steel core introduced in a concrete-filled steel tube. The core was wrapped with an unbonding layer (acrylic tape). The main difference between the two typologies refers to the way the core is obtained. For the first typology (A) the core is obtained by milling of a steel plate, which assures a smooth transition from the plastic to the elastic cross-section. Two stiffeners are welded at each end to provide stability for the elastic zone. In the case of the second BRB typology (B) the core is obtained by welding core extension plates and stiffeners to each end of a compact hot-rolled square steel profile.

The main mechanical characteristics of the BRBs investigated within this article are summarized in Table 1: area of the plastic zone of the core, $A_{p,m}$, computed using mean values of the measured geometry; plastic resistance of the BRB, $N_{p,m}$, computed using $A_{p,m}$ and the mean yield strength of the steel of the core, R_{eH} (Table 2); critical elastic force of the BRM, N_{cr}; loading protocol having the first cycle starting in tension, T, or compression, C; core to concrete gap (unbonding layer) for the through thickness, g_t, and the through width, g_w, directions with respect to the core.

Tensile tests were performed to determine the mechanical properties of the steels used to manufacture the core of the BRBs. Therefore, three identical coupons specimens were extracted parallel with the direction of lamination from the each of the core material. The mean values of the mechanical characteristics obtained are summarized in Table 2: upper yield strength, R_{eH}, tensile strength, R_m, percentage elongation after fracture, A, over-strength factor of the material, g_{ov}. All the tensile tests results comply with the product standard except for C45 material. Cyclic tests were also performed on hourglass coupons extracted from C30 steel material in order to obtain the input parameters for FEM analyses.

Type	ID	Geometry
A	CR33, CR73	
B	CS33, CS73	
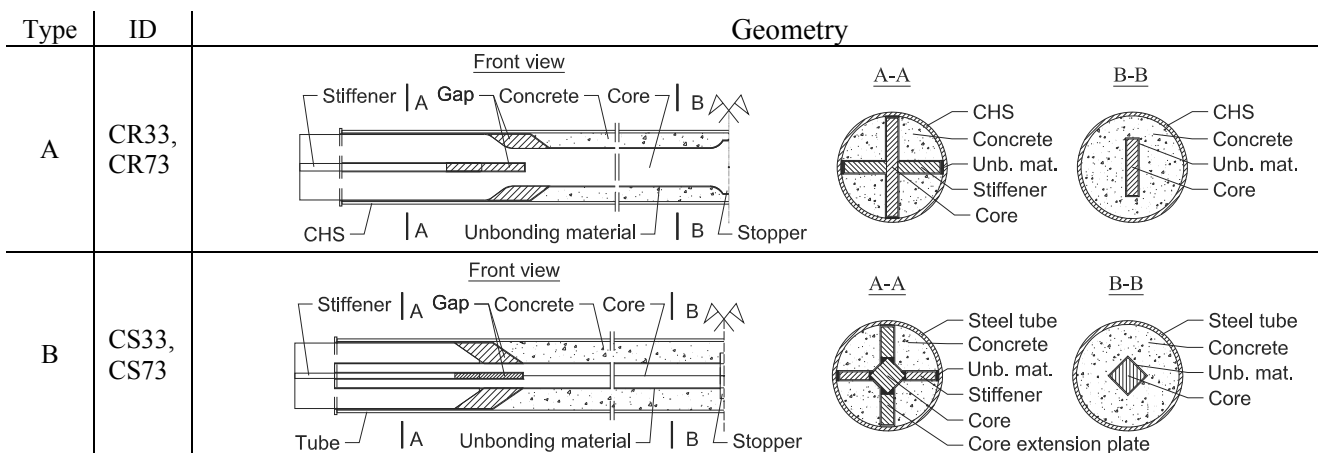
Fig. 1 – The conceptual geometry of the "conventional" BRBs.

Table 1

Experimental program: "conventional" BRBs

Type	ID	$A_{p,m}$ [mm²]	$N_{p,m}$ [kN]	N_{cr} [kN]	$N_{cr}/N_{p,m}$	Loading protocol	Unbonding material	Gaps [mm] g_t	g_w
A	CR33-1	868.3	345.4	873	2.53	T	acrylic tape	2	2
	CR33-2	868.3	345.4	881	2.55	C	acrylic tape	2	2
	CR73-1	2011.7	722.0	2093	2.95	T	acrylic tape	2	3
	CR73-2	2011.7	722.0	2102	2.91	C	acrylic tape	2	3
B	CS33-1	909.0	331.0	882	2.66	T	acrylic tape	2	2
	CS33-2	909.0	331.0	897	2.70	C	acrylic tape	2	2
	CS73-1	2007.0	565.6	2092	3.70	T	acrylic tape	2	2
	CS73-2	2007.0	565.6	2083	3.69	C	acrylic tape	2	2

Table 2

Results on tensile test

BRB ID	Core material	Product standard			Quality certificate			Tensile test			γ_{ov}
		R_{eH}, N/mm²	R_m, N/mm²	A, %	R_{eH}, N/mm²	R_m, N/mm²	A, %	R_{eH}, N/mm²	R_m, N/mm²	A, %	
CR33	C14	355	470-630	22	N/A	N/A	N/A	398	513	36.2	1.12
CR73	C20	345	470-630	22	358	508	33.1	359	510	34.7	1.04
CS33	C30	345	470-630	22	384	600	25.4	364	525	30.6	1.06
CS73	C45	335	470-630	21	353	498	30.0	282	442	35.3	0.84

3. CALIBRATION OF MATERIAL MODEL

Metal plasticity can be modelled using several approaches implemented in Abaqus 6.14 [11]. The plastic hardening behaviour can be defined using one of the available options: isotropic, kinematic, Johnson-Cook, user, combined. The first two models are relatively simple with respect to the other from the perspective of the calibration process of the input parameters. Johnson-Cook and user material will not be discussed within this paper. The combined option is a complex material model that requires a good understanding of plastic hardening in order to calibrate the material parameters. The three models will be further discussed.

The isotropic hardening model assumes the von Misses yield surface to having a fixed center, while the yield surface can increase (hardening) or decrease (softening) in shape. This model is suitable for FEM analyses where the direction of the principal stresses (σ_1, σ_2, σ_3) does not change significantly. The input parameters, yield stress-plastic strain data pairs, can be easily obtained from a uniaxial tensile test. As can be observed in Fig. 2a a good prediction for the monotonic uniaxial tensile test can be obtained with this material model. When applying cyclic loading, the prediction is inaccurate Fig. 2b.

The kinematic model assumes the yield surface having a fixed surface, while moving with a certain slope (constant rate of strain hardening) through the stress space. Since only one hardening slope can be provided, this model will lead to coarse predictions of the monotonic and cyclic behaviour of steel (Fig. 2).

In order to capture the main features of mild carbon steel (Bauschinger effect, cyclic hardening) the combined isotropic-kinematic hardening material represents a proper material model. It consists of a nonlinear kinematic hardening component (used to simulate the Bauschinger effect) and an isotropic component (used to simulate the cyclic hardening) which can be linear, multilinear, or nonlinear, depending on the input type. The calibration of the input parameters requires uniaxial cyclic test data and the procedure is described in [11]. As can be observed in Fig. 2a and b acceptable predictions can be obtained for both monotonic and cyclic loading. It needs to be mentioned that the combined model has several limitations. The most important one is the fact that the material is history dependent and it will be further discussed.

As suggested in [11], the calibration of the input parameters of the combined material model should be done using experimental results from tests having similar loading history with the tested structure. Since all the BRBs were tested using a variable loading protocol, the calibration of the steel material model resumes to the calibration of a strain-controlled cyclic uniaxial coupon test with variable strain amplitudes of ±1%, ±3%, ±5%, ±7%, and continued with cycles at ±5% until failure occurred. The calibrated material model reproduces with an acceptable level of accuracy both phases of the uniaxial cyclic test, FEM-c (Fig. 3b). The calibrated parameters were also used to simulate a monotonic tensile test, FEM-m, performed on a specimen similar to the cyclically tested ones (thus a fracture strain $\varepsilon_r = 60\%$ was reached). Acceptable predictions were obtained up to ultimate strain (Fig. 3a).

The calibration of input parameters of the kinematic hardening component of material model used to simulate the core of the BRBs is summarized in Table 3 and graphically presented in Fig. 4 (a). σ_0 is the yield stress and zero plastic strain, C_k are the values of the kinematic hardening moduli and γ_k their corresponding decreasing rate with respect to increasing plastic deformation. Since the cyclic hardening component (Fig. 4b) is dependent on the loading history, the input cannot generally be used with good predictions for modelling specimens subjected to different loading histories.

An isotropic elastic material model was chosen to simulate the behaviour of the concrete parts. An elastic modulus E_c = 20 MPa and a Poisson's ratio υ = 0.2 described the elastic behaviour. This material model reduces the material nonlinearity of the BRB model and assures fast convergence, thus considerably reducing the computational time.
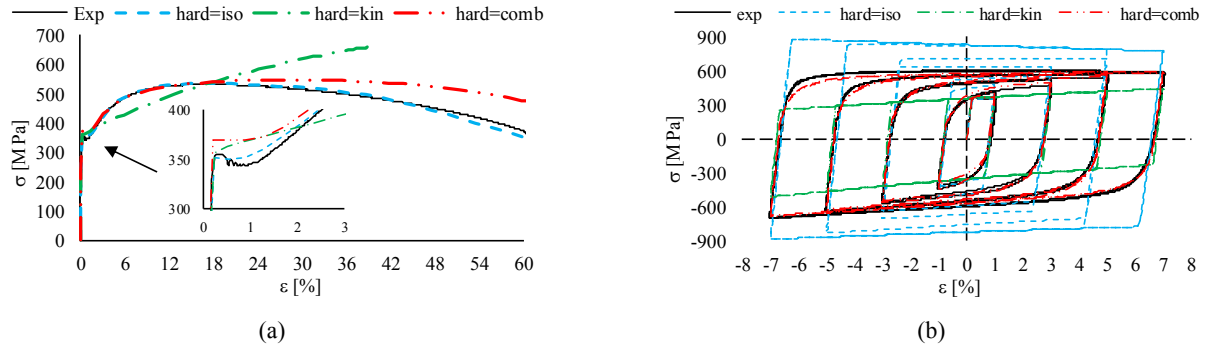
Fig. 2 – Monotonic (a) and cyclic (b) response of several numerical models vs. experimental results.
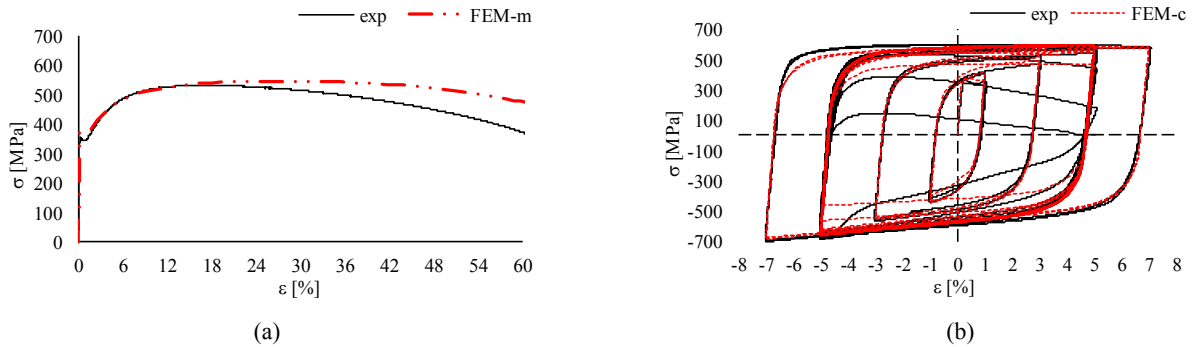
Fig. 3 – Calibrated monotonic (a) and cyclic (b) response of C30 material.
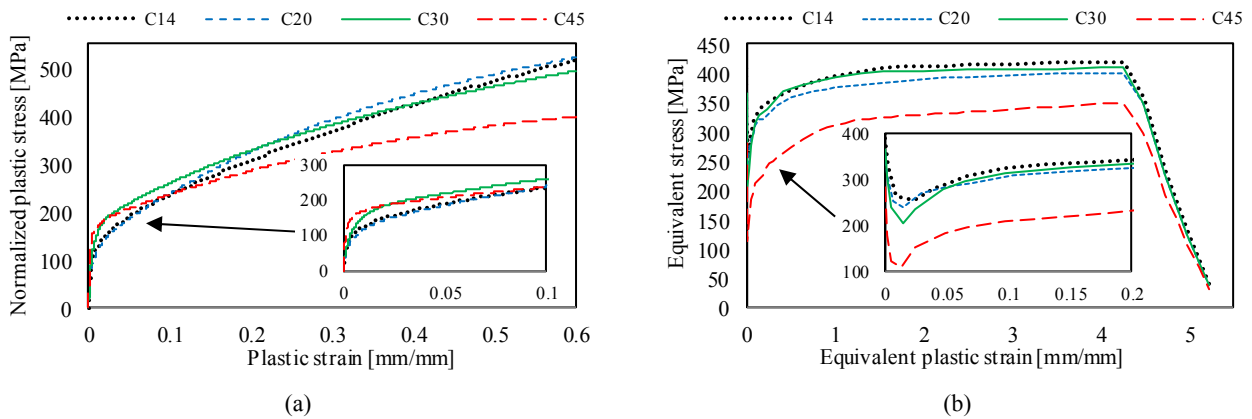
Fig. 4 – Graphical representation of the calibrated material inputs: kinematic (a) and isotropic (b) components.

Table 3

Input parameters for kinematic hardening component of the steel model

Material	σ_0	C_1	γ_1	C_2	γ_2	C_3	γ_3	C_4	γ_4	C_5	γ_5
C14	407.77	45000	850	12600	245	1900	35	630	1.3	210	1
C20	359.46	40000	900	10000	195	2000	67	950	3.5	350	1
C30	367.08	41513	697	15152	137.5	600	4.6	255	2.2	195	0
C45	282.13	95000	1300	40500	680	5000	120	500	2.5	200	2

4. BRB NUMERICAL FEM MODEL

General description of the BRB FEM model are presented in Fig. 5. All the BRB models have several common features: types of finite elements, type of material model, boundary conditions, geometrical nonlinearities, contact laws. The differences between the models relate to geometry and material input.

BRB type A

BRB type B

Common boundary conditions and loads

1 – Core: mesh size 10 & 20 mm; C3D8I; steel – combined kinematic-isotropic hardening material.
2 – Stopper: mesh size 10 mm; C3D8I; steel – combined kinematic-isotropic hardening material.
3 – Stiffener: mesh size 20 mm; C3D8I; steel – combined kinematic-isotropic hardening material
4 – Core extension plate: mesh size 20 mm; C3D8I; steel – combined kinematic-isotropic hardening material
5 – Concrete: mesh size 20 mm; C3D8R; concrete material – elastic.
6 – Tube: mesh size 20 mm; S4R; steel– combined kinematic-isotropic hardening material.
7 – Unbonding interface: gap + contact law (normal "Hard"; tangential "Penalty").
   Core-to-concrete gap: through thickness, g_t, and through width, g_w, directions.
8 – Gap for compression stroke, $L_G = 70$ mm.
9 – Contact law: concrete-to-tube composite effect (normal-hard, tangential-penalty, friction coefficient 0.4).
10 – Support 1: pinned in gravity plane ($U_x = U_y = U_z = UR_y = UR_z =$ constrained; $UR_x =$ free;
       $U_i =$ translational degree of freedom, axis i; $UR_i =$ rotational degree of freedom, axis i).
11 – Support 2: roller ($U_x = U_y = UR_y = UR_z =$ constrained; $UR_x =$ free; $U_z =$ applied cyclic loading).
12 – Gravity load: decomposed on G_y and G_z components to account for the BRB position in the experimental set-up.

Fig. 5 – FEM model of BRB.

The core of the BRB was modelled using incompatible mode eight-node linear brick elements, C3D8I, which are appropriate to model bending with contact interactions. A finer mesh was assigned to the plastic zone (10mm), while a coarser mesh for the elastic zones (20mm). The concrete was modelled using eight-node linear brick elements with reduced integration and hourglass control, C3D8R, with a global mesh size of 20 mm. The steel tube and the caps were modelled using a four-node doubly curved thin or thick shell with reduced integration, hourglass control and finite membrane strains, S4R, due to their reduced thickness, with a global mesh size of 20 mm. The unbonding material was modelled using a core-to-concrete gap and a contact law. The size of the gaps was similar to the thickness of the unbonding material applied. Gaps for compression stroke equal to 70 mm were provided in extension to the transition zones of the core to allow free movement of the core under compression loading.

A general contact was defined and the contact domain consisting of two selected surface pairs that were assigned different contact properties as follows: the core–to–concrete interaction was defined as having the tangential behaviour defined as "Penalty" with the friction coefficient calibrated based on tests (see section 5) and the normal behaviour set to "Hard" contact. The steel casing-to-concrete interaction had the same properties except that the friction coefficient which was set to 0.4. In both cases the metallic surfaces were considered "master" in the contact formulation to avoid excessive penetrations and numerical errors. Also, a coupling constraint was defined at each end of the core, by connecting a reference point to the end surface of the core using the "Kinematic" coupling type.

The BRB models had pinned supports only in the plane of the gravity force, while the other degrees of freedom were blocked. The loads, gravity and cyclic loading, were applied in two Dynamic Explicit steps. In the first step, the gravity load was applied in the *YZ* plane using a smooth step amplitude to avoid dynamic effects, and it was kept constant in the second step were the cyclic loading was applied as displacement control using the Dynamic Explicit procedure and smooth step amplitude function to assure a quasi-static analysis. The BRBs were cyclically loaded using the experimental protocol [9] but limited to 13 cycles.

The output energies were checked to validate the numerical model: kinetic energy was under 1% of the internal energy, thus assuring a quasi-static analysis; artificial energy was also low, under 1% of the internal energy, thus validating the finite elements used (no shear locking of hourglass deformation modes of the elements). External work and internal energy had an almost similar path throughout the analysis, thus validating the results obtained. Initial geometrical imperfections were modeled by using the first buckling mode of the BRB model, whose deformed shape was in the plane of the gravity load. The deformed shape was scaled so as to obtain an initial bow imperfection of 1/1000 of the length of the BRB.

5. UNBONDING INTERFACE

Since the unbonding layer was not explicitly modeled but by using a gap and a contact law, therefore it comes necessary to determine the appropriate value for the friction coefficient that describes the tangential behavior of the contact law. For this calibration, the BRB specimen CS33 was chosen due to the fact that the material used to model the core was calibrated based on experimental test data and does not represent an unknown variable. Also, to determine the friction coefficient properly, the gap size was considered equal to the thickness of the applied unbonding material. Several values for the friction coefficient were considered: 0.05, 0.1, 0.2, 0.3. As can be observed in Fig. 6 the best fit was obtained using the value 0.1. Also, the higher the friction (0.2 or 0.3), the higher is the compression overstrength and less ductile is the BRB. Using less friction (0.05) leads to lower compression overstrength and no fracture occurs, contrary to the experiment. Therefore, a value of the friction coefficient equal to 0.1 in combination with gap sizes corresponding to effective dimensions of the applied unbonding material was considered to be appropriate to model the unbonding interface.
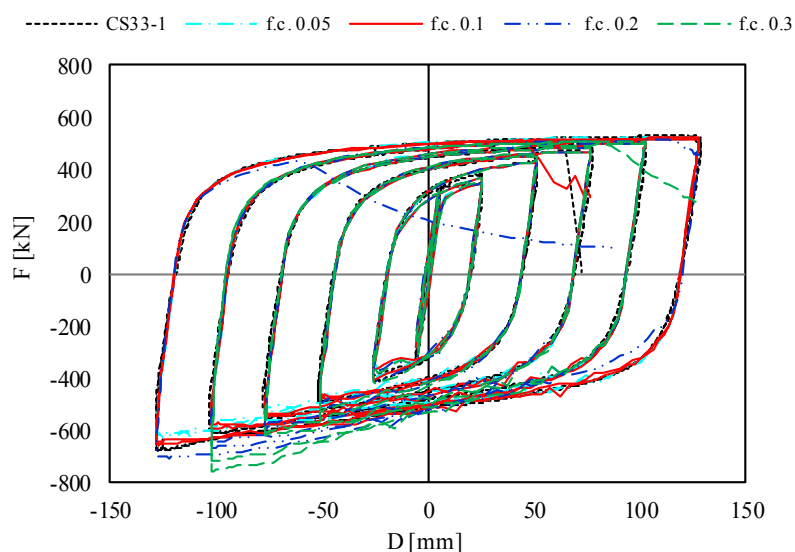
Fig. 6 – Calibration of friction coefficient for specimen CS33-1.

6. CALIBRATED BRB FEM MODELS

The calibrated parameters were used in the BRB FEM models and cyclic analyses were performed. The predictions are presented in Fig. 7. As a general observation, the numerical models were capable of reproducing with a good accuracy the experimental results. The failure mode was captured for some models (CR33, CS33), while for the others (CR73, CS73) further investigations are required. It is to be mentioned that failure of the material due to low-cycle fatigue was not explicitly included in the material model.

In case of CR33 specimens good predictions were obtained for both specimens. The hardening response at large deformations in compression was caused by increasing of the cross-sectional area of the core as a result of the Poisson's effect under compression. The increase took place mainly in the through-width direction of the plastic segment of the core, being located near the transition zones.

In case of CR73 specimens there are minor differences between FEM and experimental results. Also, between the two experimental results (CR73-1 and CR73-2) are minor differences, due to unknown reasons. Since only 12 cycles were used within the FEM simulations and the experimental specimens could sustain up to 25 cycles, the failure was not captured.

In the case of CS33 specimens the FEM models were able to predict with a good level of accuracy both the cyclic response and the failure mode.

In the case of CS73 specimens there are some differences between the experimentally obtained hysteresis loops as a cause of the imperfections due to manufacturing (misalignment of the core components). The numerical models were able to capture the cyclic behavior with an acceptable level of accuracy. Also, the fracture was properly predicted in case of CS73-2 specimen.
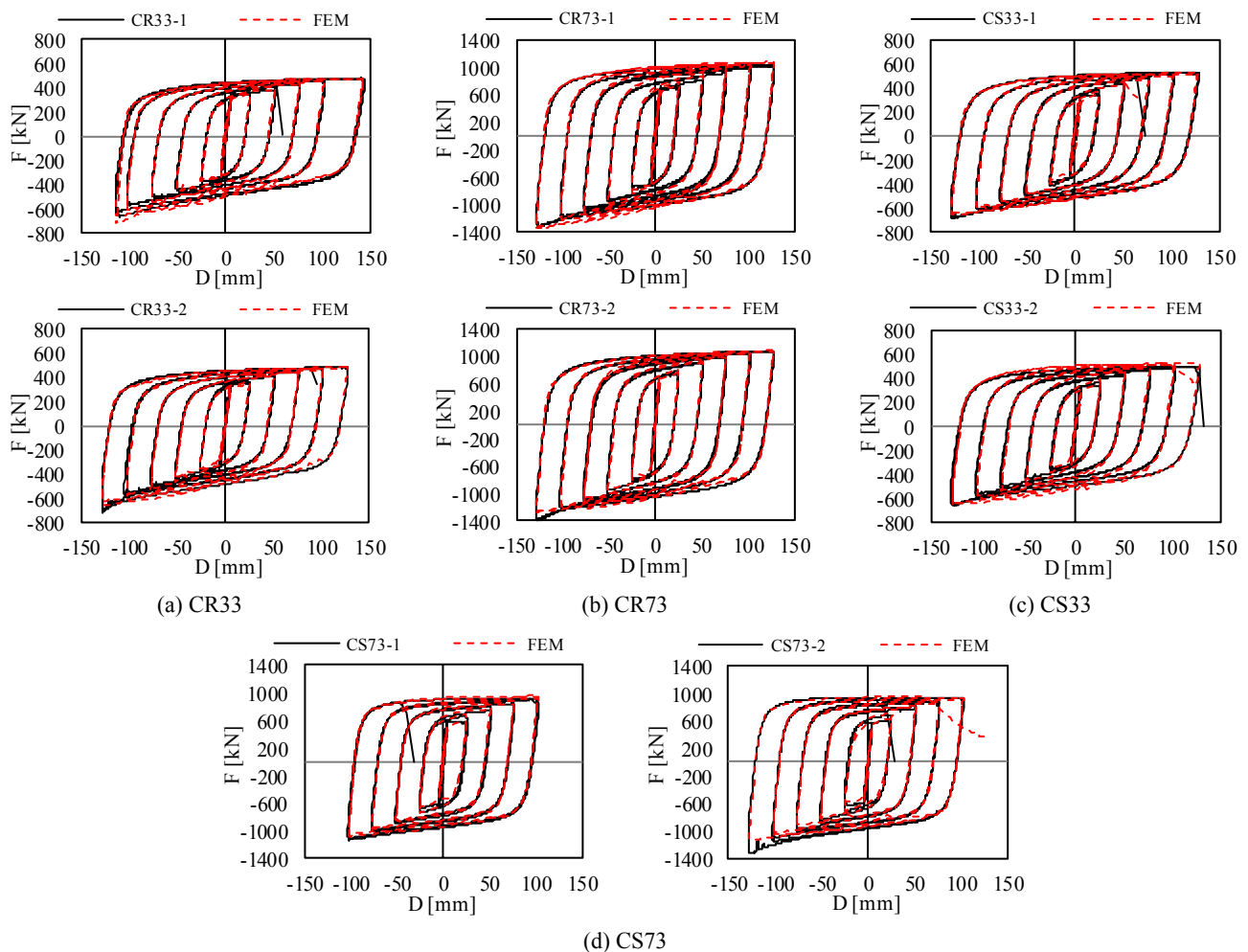
Fig. 7 – Calibration of FEM BRB models based on experimental results.

7. CONCLUSIONS

Within this paper a numerical finite element model was developed and calibrated using experimental data for a set of buckling restrained braces. Calibration was performed at material and element level.

At the material level, three models were investigated in order to assess their monotonic and cyclic predictions when simulating metal plasticity. It was confirmed that using the combined kinematic-isotropic material model acceptable predictions are obtained both under monotonic and cyclic loading. The material input was adjusted in order to better capture the cyclic behavior under variable load amplitudes. The material input for the isotropic component is dependent on the loading history. Therefore, the calibration should be done using a uniaxial coupon test with a loading history similar to the one experienced by the material in the modelled structure (BRB).

The unbonding material can be properly modeled using a gap and a contact law. For steel core to concrete interaction, a size of the gap equal to the nominal thickness of the unbonding layer and a contact law with the tangential behavior having a friction coefficient equal to 0.1 led to good agreement with the experimental results.

Four FEM BRB models corresponding to the two typologies (rectangular core - type A, square core - type B), and to the two capacities (300 kN 700 kN) were developed. Cyclic numerical analyses were performed on these models and good predictions with respect to experimental results were obtained.

The calibrated BRB FEM model will be further used to assess the influence different parameters on the cyclic performance of the qualified BRBs.

ACKNOWLEDGEMENTS

REFERENCES

1. Q. XIE. *State of the art of buckling-restrained braces in Asia*, Journal of Constructional Steel Research, **61**, *6*, pp. 727–748, 2005.
2. A. WATANABE, Y. HITOMI, E. SAEKI, A. WADA, M. FUJIMOTO. *Properties of brace encased in buckling restraining concrete and steel tube*, Proc. 9th World Conf. Earthquake Engineering, **4**, pp. 719-724, 1988.
3. M. D'ANIELLO, G. DELLA CORTE, F.M. MAZZOLANI, *'All-steel' buckling-restrained braces for seismic upgrading of existing reinforced concrete buildings*, in Proc. STESSA 2009 (Behaviour of Steel Structures in Seismic Areas), 2009.
4. S. BORDEA. Dual frame systems of buckling restrained braces, PhD Thesis, Timişoara, 2010.
5. L. DUNAI, A. ZSARNÓCZAY, L. KALTENBACH, M. KÁLLÓ, M. KACHICHIAN, A. HALÁSZ. *Type testing of Buckling Restrained Braces according to EN 15129 – EWC800*, Final report, 2011.
6. EUROPEAN COMMITTEE FOR STANDARDIZATION (CEN), *Design of structures for earthquake resistance. Part 1: General rules, seismic actions and rules for buildings*, Eurocode 8-1/2008.
7. EUROPEAN COMMITTEE FOR STANDARDIZATION (CEN), *Anti-seismic devices*, EN 15129, 2010.
8. MINISTRY OF REGIONAL DEVELOPMENT AND PUBLIC ADMINISTRATION, *Code for seismic design. Part I. Design prescriptions for buildings,* P100-1/2013.
9. A. STRATAN, C.I. ZUB, D. DUBINĂ, *Experimental Tests for Pre-Qualification of a Set of Buckling-Restrained Braces*, Key Engineering Materials, **763**, pp. 450–457, in Proc. STESSA 2018 (Behaviour of Steel Structures in Seismic Areas), 2018.
10. AMERICAN INSTITUTE OF STEEL CONSTRUCTION, *Seismic Provisions for Structural Steel Buildings*, ANSI/AISC 341-10, Inc. Chicago, Illinois, USA, 2010.
11. ABAQUS, FEA, *ABAQUS 6.14 Documentation*, Dassault Systemes, Providence, RI, USA, 2014.